Relativistic Quantum Mechanics Applications Using The Time Independent Dirac Equation In COMSOL

A. J. Kalinowski[*1]
[1]Consultant
*Corresponding author: East Lyme CT 06333, kalinoaj@aol.com

Abstract: COMSOL is used for obtaining the quantum mechanics wave function $\{\Psi_m(x,y,z,t)\}$ as a solution to the *time independent* Dirac equation. The probability determination of a particle being at a spatial point can be treated by a) the "matrix mechanics formulation" or b) the "wave function formulation". The latter approach is used herein, because it involves solving field partial differential equations, thus is directly adaptable to COMSOL.

Keywords: Quantum Mechanics, Time Independent Dirac Equation, Wave Propagation.

1. Introduction

The purpose of this paper is to illustrate the use of COMSOL for obtaining the quantum mechanics wave function $\{\Psi_m(x,y,z,t)\}$ (representing *matter waves*) as a solution to the *time independent* Dirac equation. In quantum mechanics, solutions for the probability of a particle being at a particular point in space are usually treated through: a) the "matrix mechanics formulation" originated by Werner Heisenberg or b) the "wave function formulation" originated by Erwin Schrödinger. The latter approach is the one used herein, mainly because it involves solving field partial differential equations, and therefore is directly adaptable to COMSOL.

The Dirac equation is employed in particle physics and historically provided the first combined application of quantum mechanics and relativity theory by introducing a four component wave function $\{\Psi_m\}$ m=1,2,3,4 (e.g. in contrast to the one component Schrödinger wave function Ψ). Historically, $\{\Psi_m\}$ described the behavior of fermion type particles (e.g., electrons) and further predicted the existence of antiparticles (e.g., positrons) even before they were observed experimentally. Use of COMSOL MULTIPHYSICS®: the Coefficient-Form PDE "time independent" study is employed. When the wave vector **k** lies in the xy plane, the 4 component $\{\Psi_m\}$ simplifies into two components for m=1&4. COMSOL is then used for obtaining the 2-D wave function $\{\psi_1(x,y,\omega),\psi_4(x,y,\omega)\}$ as a solution to the exp(-iωt) time varying steady state Dirac equation at frequency ω.

There are multiple examples in the COMSOL archives for solving the Schrödinger wave function; however, this appears to be the first COMSOL application towards solving the Dirac equation wave function. Thus we first proceed with three validation examples (using comparisons to exact solutions), followed by an example without an exact solution available.

2. Governing Equations

Governing equations for the behavior of a free fermion particle of mass *m* are represented by the *time dependent* quantum mechanics Dirac equations (with wave function $\{\Psi_m(x,y,z,t)\}$ as the dependent variables) and are given by [1]:

$$\frac{1}{c}\frac{\partial \Psi_1}{\partial t} + \frac{\partial \Psi_4}{\partial x} - i\frac{\partial \Psi_4}{\partial y} + \frac{\partial \Psi_3}{\partial z} + iM'\Psi_1 = 0$$
$$\frac{1}{c}\frac{\partial \Psi_2}{\partial t} + \frac{\partial \Psi_3}{\partial x} + i\frac{\partial \Psi_3}{\partial y} - \frac{\partial \Psi_4}{\partial z} + iM'\Psi_2 = 0 \quad (1)$$
$$\frac{1}{c}\frac{\partial \Psi_3}{\partial t} + \frac{\partial \Psi_2}{\partial x} - i\frac{\partial \Psi_2}{\partial y} + \frac{\partial \Psi_1}{\partial z} - iM'\Psi_3 = 0$$
$$\frac{1}{c}\frac{\partial \Psi_4}{\partial t} + \frac{\partial \Psi_1}{\partial x} + i\frac{\partial \Psi_1}{\partial y} - \frac{\partial \Psi_2}{\partial z} - iM'\Psi_4 = 0$$

with M'=mc/$\hbar$, c= speed of light, $\hbar$ =h/(8π), (where *h* is Plank's constant), and $i = \sqrt{(-1)}$.

3. Method

The governing Eqs.(1) are solved for both Eigenvalue and for steady state problems using the COMSOL MULTIPHYSICS® Coefficient-Form PDE "Eigenvalue" and the "T*ime Independent*" studies. Two dimensional solutions are sought where the wave function depends on spatial coordinates x,y. Therefore gradients in the

z direction drop out and the uncoupled { $\Psi_1(x,y,t), \Psi_4(x,y,t)$ } components are solved with just the first and fourth equations of Eqs.(1).

3.1 Eigenvalue Problem: Cartesian Coord.

Solutions are sought of the form:

$$\Psi_m = \psi_m (x,y)\, exp(-\lambda't) \qquad (2)$$

and upon substituting Eq.(2) into the first and fourth of Eqs.(1), one obtains:

$$\begin{bmatrix} icM' & c\left(\frac{\partial}{\partial x} - i\frac{\partial}{\partial y}\right) \\ c\left(\frac{\partial}{\partial x} + i\frac{\partial}{\partial y}\right) & -icM' \end{bmatrix} \begin{Bmatrix} \psi_1 \\ \psi_4 \end{Bmatrix} = \underset{i\omega}{\lambda'} \begin{Bmatrix} \psi_1 \\ \psi_4 \end{Bmatrix} \quad (3)$$

as the standard Eigenvalue form. With homogenous boundary conditions, we seek the Eigenvalue λ'_n and associated N Eigenvectors { $\psi_1(x,y, \lambda'_n)$, $\psi_4(x,y, \lambda'_n)$ }$_n$, n=1,2,...N that satisfy Eq.(3).

3.2 Steady State Problem: Cartesian Coord.

Solutions are sought of the form:

$$\Psi_m = \psi_m (x,y)\, exp(-i\omega t) \qquad (4)$$

and upon substituting Eq.(4) into the first and fourth of Eqs.(1), one obtains:

$$\frac{\partial \psi_4}{\partial x} - i\frac{\partial \psi_4}{\partial y} + i(M' - \omega/c)\psi_1 = 0 \qquad (5)$$
$$\frac{\partial \psi_1}{\partial x} + i\frac{\partial \psi_1}{\partial y} - i(M' + \omega/c)\psi_4 = 0$$

as the steady state Cartesian coord. form. With non-homogenous B.C.'s (Boundary Conditions), the boundary is driven, and solutions {$\psi_1(x,y,\omega)$, $\psi_4(x,y,\omega)$ } are sought that meet Eqs.(5).

3.3 Eigenvalue Problem: Cylindrical Coord.

Solutions are sought of the form:

$$\Psi_m = \psi_m (\rho,\varphi)\, exp(-\lambda't) \qquad (6)$$

where upon substituting Eq.(6) into the cylindrical coordinate form [2] of the first and fourth of Eq.(1) (after correcting a missing i factor in Eqs.(28) and 29 of [2]) one obtains:

$$\begin{bmatrix} icM' & ce^{-i\varphi}\left(\frac{\partial}{\partial \rho} - \frac{i}{\rho}\frac{\partial}{\partial \varphi}\right) \\ ce^{+i\varphi}\left(\frac{\partial}{\partial \rho} + \frac{i}{\rho}\frac{\partial}{\partial \varphi}\right) & -icM' \end{bmatrix} \begin{Bmatrix} \psi_1 \\ \psi_4 \end{Bmatrix} = \underset{i\omega}{\lambda'} \begin{Bmatrix} \psi_1 \\ \psi_4 \end{Bmatrix} \quad (7)$$

as the cylindrical coordinate Eigenvalue form, where ρ and φ are the conventional radial and angular coordinates. With homogenous boundary conditions, the eigenvalue λ'_n and associated N eigenvectors { $\psi_1(\rho,\varphi, \lambda'_n)$, $\psi_4(\rho,\varphi, \lambda'_n)$ }$_n$, n=1,2, ...N are sought that satisfy Eq.(7).

3.4 FEM Solutions: Cartesian Coord.

The Coefficient-Form PDE "*Time Independent*" Study is used for Eigenvalue and steady state type problems and are used to solve the example models presented herein.
Element Type: "Free Quadratic" elements are used for mesh generations with quadratic shape functions.
Boundary Condition Enforcement: Constraint Enforcements of the form:

$$R_m(\psi_m, \frac{\partial \psi_m}{\partial x}, \frac{\partial \psi_m}{\partial y}) = 0 \qquad (8)$$

are employed, where the "*Apply Reaction Terms On*" option of "*Individual Dependent Variables*" is selected; also the "*Use Weak Constraints*" box is checked "*On*". This combination worked out for the field equations solved herein.
Element Size: The examples treated here involve propagating waves (of spatial wavelength λ), and therefore the maximum element size is limited by $(\Delta L)_{max} \leq \lambda/12$. For regions involving an expected higher degree of spatial response change, an even finer mesh was employed such as in the last two-slit example FEM solution.

4. Theory

The basic building blocks of the Dirac theory are freely propagating matter waves such as planar and cylindrical ones. The treatment of simulating infinite domains with truncated finite domains by using absorbing boundary conditions is discussed.

4.1 Plane Waves

The exact solution to Eq.(3) for a plane wave of freq. ω traveling in unit vector direction **n,** (with position vector **r**=x**i**+y**j**), is given by [1] :

$$\begin{Bmatrix} \psi_1 \\ \psi_4 \end{Bmatrix} = A \begin{Bmatrix} 1 \\ \dfrac{exp[i\theta_{inc}]}{R} \end{Bmatrix} exp[ik\hat{\rho}] \quad ; \hat{\rho} = \vec{n} \cdot \vec{r} \quad (9)$$

$$\lambda' = i\omega; \;\; k = \sqrt{(\omega/c)^2 - M'^2}; R = \frac{k}{(\omega/c) - M'} \quad (10)$$

where A is an arbitrary constant. As an example, for a plane wave traveling in the +x direction, set

n= x**i**, $\theta_{inc}=0$, thus $\hat{\rho}$=x; whereas for a wave in the -x direction, set **n**= -x**i**, $\theta_{inc}=\pi$, thus $\hat{\rho}$=-x.

4.2 Cylindrical Waves

Exact solutions to Eq.(7) representing cylindrical waves traveling in the radial unit vector direction $\mathbf{n_\rho}$ are given by [3] :

$$\begin{Bmatrix} \psi_1 \\ \psi_4 \end{Bmatrix} = A' \begin{Bmatrix} H^{(1)}_{([n-1]/2)}(k\rho)\,exp[i\varphi(n-1)/2] \\ \frac{i}{R} H^{(1)}_{([n+1]/2)}(k\rho)\,exp[i\varphi(n+1)/2] \end{Bmatrix} \approx \quad (11)$$

$$A'' \left\{ \frac{1}{R} exp[i\varphi] \right\} \frac{exp[ik\rho]}{\sqrt{k\rho}} exp[i\varphi(n-1)/2]\ \ n=1,3,5,...$$

$$\lambda' = i\omega;\ \ k=\sqrt{(\omega/c)^2 - M'^2};\ R=\frac{k}{(\omega/c)-M'}\ (12)$$

where the H terms are Hankel functions of the first kind, A′, A″ are arbitrary constants, and the odd n=1,3,5… correspond to a set of Eigenfunctions. The second approximate solution above is for large Bessel function arguments, kρ≫1. We seek the simplest wave structure that looks like a plane wave, except for a spreading reduction term in the ρ direction. Thus for n=1, the 2nd of Eqs.(11) reduces to:

$$\begin{Bmatrix} \psi_1 \\ \psi_4 \end{Bmatrix} = A'' \left\{ \frac{1}{R} exp[i\varphi] \right\} \frac{exp[ik\rho]}{\sqrt{k\rho}} \qquad (13)$$

which looks like the plane wave solution Eq.(9) (except for the $1/\sqrt{k\rho}$ spreading loss factor) and the angle of incidence term θ_{inc} corresponds to the cylindrical coordinate φ. The cylindrical solution acts like a set of local plane waves emanating from a boundary ρ=constant.

4.3 Absorbing Boundary Condition

When a plane or cylindrical wave travels outward and encounters an artificial cut into a modeled infinite domain, an absorbing boundary condition is needed to properly terminate the FEM mesh. The constraints shown next are enforced as a special case of Eq.(8).
Plane Wave Absorber: by differentiating Eq.(9) in the direction of propagation, e.g. +x, a relation between ψ_m and $\partial\psi_m/\partial x$ can be obtained:
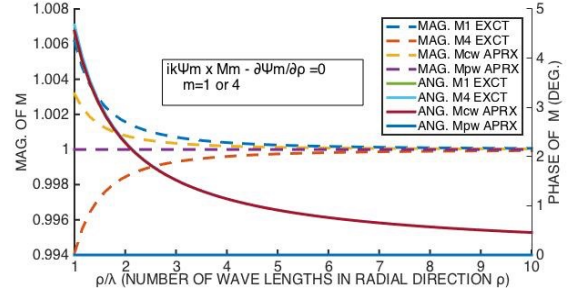
$$ik\psi_m - \frac{\partial\psi_m}{\partial x} = 0 \qquad (14a)$$

and similarly for a wave traveling in the -x direction, the boundary condition is:

$$ik\psi_m + \frac{\partial\psi_m}{\partial x} = 0 \qquad (14b)$$

Cylindrical Wave Absorber: by differentiating Eq.(13) in the direction of propagation, e.g. +ρ, a relation between ψ_m and $\partial\psi_m/\partial\rho$ can be obtained:

$$ik\psi_m\left(1+i/2\rho k\right) - \frac{\partial\psi_m}{\partial\rho} = 0 \quad (15)$$

Figure 1. Cyl. Wave Absorbing Boundary Condition Compared to Plane Wave Boundary Condition

The Fig.(1) absorber comparisons show that after placing the B.C. cut around $\rho/\lambda \geq 3$ wave lengths from the origin, the cylindrical absorber coefficient M_m approaches the plane wave absorber M_m in both amplitude and phase. The curves labeled M_m EXCT and ANG. M_m EXCT are obtained from the first of Eqs.(11) for n=1.

4.4 Over Constrained Spatial Boundary Cond.

A simple 1-D example illustrates care must be taken regarding what is used for the boundary conditions downstream of the wave propagation. The advection equation is both 1st order in space and in time, thus is a close relative to the 1-D Dirac equation that is also 1st order in space and in time. The 1-D advection equation has only 1 unknown as opposed to the 1-D Dirac equation that has 2 unknowns, thus it is simpler to explain the over constrained issue for the advection equation. Contrast the 1-D *1st order in space* and in time advection equation to the 1-D *2nd order in space* and 1st order in time Schrödinger equation. Shown below is the Eq.(16) advection equation and the Eq.(17) Schrödinger equation.

$$\frac{\partial\Psi}{\partial t} + C\frac{\partial\Psi}{\partial x} = 0\ ;\ C=wave\ speed \qquad (16)$$

$$ia\frac{\partial\Psi}{\partial t} + \frac{\partial^2\Psi}{\partial x^2} = 0\ \ ;\ a=2m/\hbar \qquad (17)$$

The steady state solution is sought, therefore upon substituting Eq.(4) into Eq.(16) and Eq.(17) and solving the remaining ordinary differential equations, one obtains:

$$\psi = B_1 exp(ikx)\ ;\qquad\qquad k=\omega/C \quad (18)$$
$$\psi = A_1 exp(ikx) + A_2 exp(-ikx)\ ;k=\sqrt{a\omega} \quad (19)$$

where Eq.(18) is the advection equation solution with only one arbitrary constant B_1 to evaluate and Eq.(19) is the Schrödinger equation solution with two arbitrary constants A_1, A_2 to evaluate. Both equations support waves traveling in the +x direction (the B_1 and A_1 terms), however Eq.(19) can support a backward traveling wave in the -x direction (the A_2 term).

The FEM Coefficient-Form PDE "time independent" *COMSOL solver requires a boundary condition to be applied at* both *ends of the domain, 0 ≤x≤ L.* Therefore when using a first order pde like the advection equation (or Dirac equation), one must use a boundary condition at the downstream end (e.g. x=L) that is consistent with what the solution would have been for the outgoing undisturbed wave. Two simple steady state illustrative examples are given next in order to illustrate the consequence of first meeting this consistency requirement and secondly not meeting the requirement.

Plane wave down infinite rod; B.C. $\psi(0)=1$

Analytic solution: in the case of the Schrödinger equation, there are two arbitrary constants, but since there is no reflected wave, A_2 =0 and A_1 is set = $\psi(0)=1$. For the advection solution, B_1 is set = $\psi(0)=1$.

Finite element solution: one cannot model infinity, so an artificial cut is made at x=L and an Eq.(14a) wave absorbing boundary condition is used to terminate the mesh. The exact vs FEM real part is shown in Figs.(2a) & (2b) for the Schrödinger and advection equation solutions respectively, where good comparisons are achieved for both plots (imag. parts also agreed).

Two end driven finite rod; B.C. $\psi(0)=1$; $\psi(L)=-2$

Analytic solution: in the case of the Schrödinger equation, A_1,A_2 are evaluated to meet the two boundary conditions at x=0 and x=L. In the case of the advection equation, only arbitrary constant B_1 is available, therefore one arbitrary constant *cannot* be selected to meet two boundary conditions at say x=0 and at x=L. We enforce $B_1=\psi(0)=1$, but one gets what the solution dictates at $\psi(L)$, not the desired $\psi=-2$.

Finite element solution: here a cut into infinity is made, thus the domain is a fixed length x=L. COMSOL demands a boundary condition at x=L (if you apply nothing there it uses default $\psi(L)=0$). Upon applying the same boundary conditions $\psi(0)=1$; $\psi(L)=-2$ to both the Schrödinger equation and the advection equation, we get the results shown in Figs.(2c) & (2d). The COMSOL Schrödinger solution matches with the exact solution, but although the COMSOL advection solution meets both BC's, there are erratic zigzag oscillations v.s. x . Note if we applied a boundary condition of

$\psi(L)=1.0\exp(ikL)$ (<u>one that is consistent with the freely propagating wave</u>), then the COMSOL and exact solution matched (this was done but results are not shown here due to space limits).
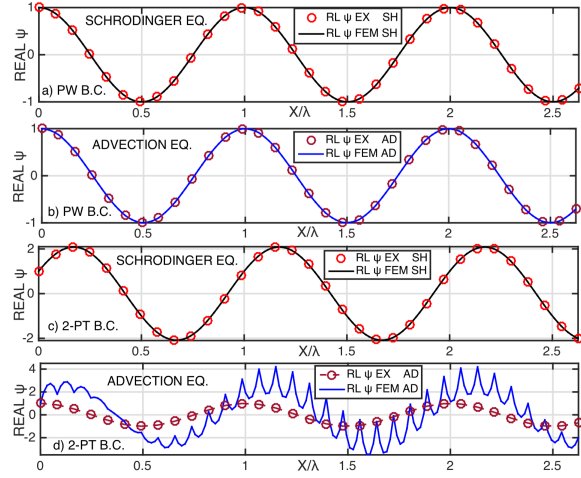
Figure 2. Solution comparison of second order in x Schrödinger equation and first order in x advection equation using the same boundary conditions

In a similar manner, care must be taken in setting the downstream boundary conditions for the Dirac first order in x equations. The use of absorbing boundary conditions to simulate infinity is used in the all COMSOL example problems to follow in this paper.

4.4 Probability Computation

The wave function $\psi_m(x,y)$ can be used to compute the probability $P_{\Delta A}$ of a particle being in a particular finite area zone, ΔA, of space for 2-D models. Firstly, the probability density $\rho'(x,y)$ is defined as the probability per unit area of the the particle being at a particular spatial point x,y and is given by Eq.(20) [1]:

$$\rho'(x,y) = |\psi_1|^2 + |\psi_4|^2 \qquad (20)$$
$$P_{\Delta A} = \Lambda \iint_{\Delta A} \rho'(x,y)\,dxdy \qquad (21)$$

The probability $P_{\Delta A}$ can be computed with Eq. (21), where the normalizing factor Λ is set so $P_{\Delta A} \rightarrow 1$ when $\Delta A \rightarrow A_{Total}$ (model total area)[4].

5. Numerical Models

The FEM models herein all use the same pde Dirac equation parameters. Length quantities are very small at the atomic level, therefore in the results presentation, length quantities are given as a multiple of the incident wave length $\lambda=2\pi/k$.

5.1 Model Parameters

All Dirac equation solutions use the following parameters in the pde's: c= 2.998e10 cm/sec, $\hbar$ =h/(8π) = 1.055e-27 erg/sec and the particle (electron) mass m = 9.109e-28 grams.

Eigenvalue models: the user enters a wave number k (via the B.C. Eq.(14a) and solves for the corresponding eigenvalue λ' (the sought after Eigenfrequency ω is extracted from λ'=i ω).

Steady state models: one face of the model is driven with a plane (or cylindrical wave) at a specific ω related to the particle velocity [1]:

$$\omega = \frac{E_p}{\hbar} = cM'/\sqrt{1-(v/c)^2} \qquad (22)$$

where E_p is the particle energy, v = 103.0e8 cm/sec is the particle velocity. It is purposely made approximately 50 times bigger than a typical electron velocity so that the strength of the *so called* [1] "ψ_4 *small component*" is not dwarfed in comparison to the "ψ_1 *large component*" for plotting contrast. Thus using Eq.(22), it follows that ω=8.26e20 rad/sec (i.e. f=1.31e20 Hz).

6. Results

Three validation models are first addressed, where the exact solution is also known, followed by a complex double slit example. Problems are solved using the section 5.1 model parameters.

6.1 Plane Wave Eigenvalue Validation

An infinite 2-D domain is modeled with a finite element zone of length L (in direction of propagation) and width W as shown in Fig.(3a) inset. The model is terminated with an Eq.(14a) forward facing absorbing boundary condition at both end faces, and B.C. $\partial\psi_m/\partial y$=0 on both lateral faces normal to the direction of propagation. The k-ω relation for a propagating wave in the x direction is sought. For a selected k, (say k=9.4544e9), the Eq.(3) is solved in COMSOL for Eigenvalue λ' (ω is the imag part of λ') and for the corresponding Eigenfunction ψ_m. The model dimensions are set as L=2.625λ x W=1λ, where λ=2π/k. While post processing the COMSOL solution, there are many Eigenvalues to sort through, however the value sought is one having a purely imaginary λ' (thus the response has a harmonically varying Eigenfunction in the x direction and is constant in the y direction). A presentation of one such solution is illustrated in Fig.(3d), where the FEM solution is shown in comparison to the exact solution (using **n**= x**i**, θ_{inc}=0 in Eqs.(9-10)). Good agreement between the two results is obtained. The exact

Eigenfrequency (from 2nd of Eqs.(10)) is ω_{EX}=8.261e20, compared to COMSOL's ω_{FEM}=8.256e20. COMSOL successfully computed the FEM amplitude ratio ≡ (max Realψ_1)/(max Realψ_4) = 5.68 compared to the EXACT amplitude ratio ≡ 1/R=5.65 . The 2-D FEM Real ψ_1 and FEM Real ψ_4 carpet plots are shown in Figs.(3b) & (3c) insets respectively.
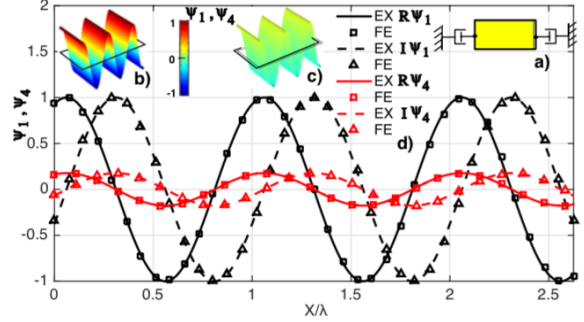
Figure 3 Wave Function Eigenvector ψ_1, ψ_4 vs. Normalized x/λ Coordinate ; (a) Simulated Infinite Domain FEM Model; (b) FEM Real ψ_1 vs. x,y; (c) FEM Real ψ_4 vs. x,y; (d) Real & Imag. ψ_1, ψ_4 of FEM ↔Exact Comparison Solutions @ Mid Line y=0

6.2 Reflected Wave Steady State Validation

A semi-infinite 2-D domain (Fig.(4a) inset) is considered where an incident plane wave arriving from x= -∞ (given by Eq.(9)) travels in the +x direction and is reflected back from a perfectly reflecting boundary condition at x=L . In scalar pde's such as the acoustic wave equation or Schrödinger equation, a reflecting boundary condition would simply be $\partial p/\partial x$ =0 or $\partial\psi/\partial x$ =0 at x=L respectively. However in the two component Dirac equation, the Eqs.(23)

$$\frac{\partial\psi_1^T(x,y)}{\partial x}\Big|_{x=L}=0 \qquad \psi_4^T(L,y) = 0 \quad (23)$$
$$where \quad \psi_m^T = \psi_m^I + \psi_m^R$$

B.C.'s will reflect a ψ_m^R wave backward with the same strength as the incident wave ψ_m^I . The exact solution that meets Eqs.(23) is given by:

$$\begin{Bmatrix}\psi_1^T\\\psi_4^T\end{Bmatrix}_{EX} = A_{inc}\underbrace{\begin{Bmatrix}1\\\frac{1}{R}\end{Bmatrix}exp[ikx]}_{INCIDENT} + A_{inc}\underbrace{\begin{Bmatrix}1\\\frac{-1}{R}\end{Bmatrix}exp[-ik(x-2L)]}_{REFLECTED}$$

where the coefficient A_{inc} is set = 1.0. The finite element model is modeled with a zone of length L and width W where the L=2.625λ x W=1λ domain size of the previous example is used. The model is terminated at end face x=L with Eqs. (23) boundary conditions and at lateral end faces

y=0 & y=W with boundary condition $\partial\psi_m/\partial y=0$. For the boundary cut into infinity at the x=0 face, there is something known (i.e. incident wave ψ^I_m using Eq.(9) at x=0) and something unknown (i.e. reflected wave ψ^R_m). Differentiating the third of Eqs.(23) and using the backward facing absorber Eq.(14b), the following Eq.(24) "drive through the absorber" boundary condition is enforced via Eq(8):

$$\underbrace{ik\psi^T_m + \frac{\partial\psi^T_m}{\partial x}}_{BACKFACING\ ABSORBER} - \underbrace{2ik\psi^I_m}_{INCIDENT\ DRIVER} = 0 \quad (24)$$

The section 5.1 steady state model parameters are used in the FEM runs and good agreement between the Total FEM vs Exact magnitude $\{|\psi|\}_T$ solutions are given in Fig.(4c) .
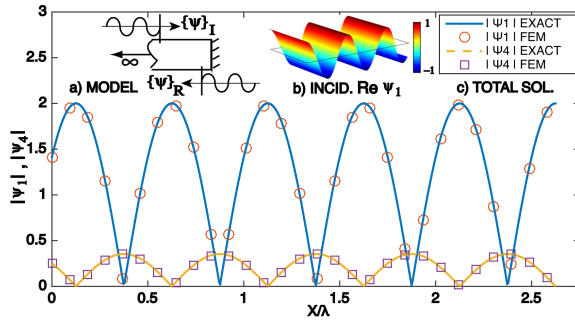

Figure 4 Interaction of Dirac Plane Wave With Reflecting Boundary: (a) Semi Infinite FEM Model, (b) 2-D Real ψ_1 FEM Incid. Wave Alone (c) FEM vs. Exact Mag. of Total Sol. $\{\psi\}_T = \{\psi\}_I + \{\psi\}_R$ vs. x/λ

The peak $\{|\psi|\}_T$ solution magnitude is double the magnitude of the incident wave which is analogous to an acoustic wave reflected from a reflecting B.C. . The Fig.(4b) inset shows what the FEM incident solution alone would look like *if it did not hit* a reflecting boundary at end x=L, where an Eq.(14a) forward absorbing B.C. was used in place of the Eqs.(23) reflecting B.C. .
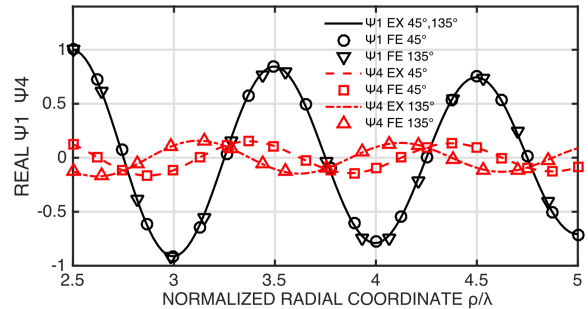
6.3 Cylindrical Wave Steady State Validation

The two previous examples were for a one dimensional wave embedded in a two dimensional space, therefore solutions varied in the x direction but were constant in the y direction of propagation. This next validation is a more complex example where the solution varies in both x and y as the wave propagation unfolds. The problem consists of a circular annular region $R_i \leq \rho \leq R_o$; $0\leq \varphi \leq 2\pi$, driven on the inner radius by the Eq.(13) cylindrical wave, evaluated at $\rho=R_i$. The outer boundary, at $\rho=R_o$, is terminated with an Eq.(15) radial absorbing

boundary condition (rewritten in Cartesian coordinates). The section 5.1 steady state model parameters are used in the FEM run, where the model size in terms of wave lengths is: $R_i =2.5\lambda$, $R_o =5.0\lambda$. Good agreement for ψ_1, ψ_4 is achieved between the FEM solution and the corresponding Eq.(13) exact solution, as shown in Fig.(5) .
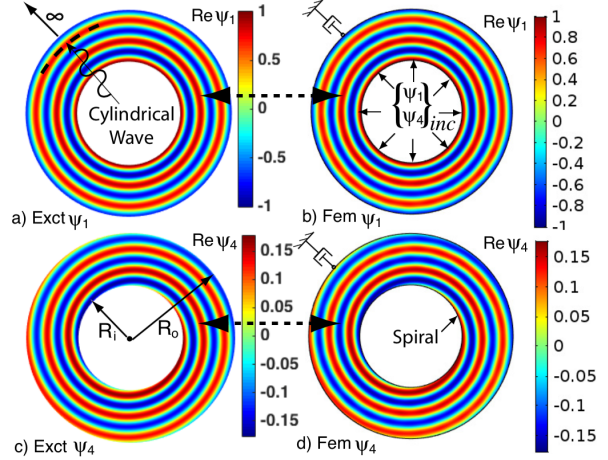
Figure 5 Dirac Cyl. Wave : (a) Exact Real ψ_1 , (b) FEM Real ψ_1 , (c) Exact Real ψ_4 , (d) FEM Real ψ_4

It is of particular interest to note that in Figs.(5c) & (5d), COMSOL successfully tracked the spiral exp(iφ) response in the ψ_4 small component wave function. Similar agreement (not shown) was obtained for plots of the imaginary component. The exact ψ_4 varies with φ, but the probability density ρ' depends on $|\psi_4|^2$ and since $|exp(i\varphi)|=1$, the probability along the ψ_4 wave front (i.e. for ρ=constant) is independent of φ .


Figure 6 Cylindrical Wave: Exact vs. FEM Real Part ψ_1, ψ_4 vs. ρ/λ for constant φ=45º and φ=135º

Comparisons for real ψ_1,ψ_4 along a ρ/λ coordinate for constant φ=45º and φ=135º fixed angles, are shown in Fig.(6), where there is good agreement between the Exact and FEM solutions. Imag. ψ_1,ψ_4 (not shown) also agreed.

6.4 Two Slit Interference Demonstration

Reference [4] treated the interference pattern set up by a *time dependent* Schrödinger equation plane wave incident upon two slits. A similar two slit problem is solved here where a steady state *time independent* Dirac equation plane wave is incident upon two slits of aperture $W=\lambda/12$, separated by a pitch of $S=2\lambda$ as shown in the Fig. (7a) inset enlargement. The FEM model is simplified herein, where an Eq.(9) Dirac plane wave is driven directly at the back of the slits, and B.C. Eq.(24) is applied there (as in problem 6.2, this back facing absorber is included in case any spurious back reflections are present from any imperfections in the outer boundary absorbing B.C.). The Eq.(15) absorbing B.C. is used at the outer model radius $R_o=5\lambda$, where Fig.(1) shows that at $\rho/\lambda=5$, the cylindrical wave B.C. is for all practical purposes like the simple plane wave absorber. An Eq.(14b) backward
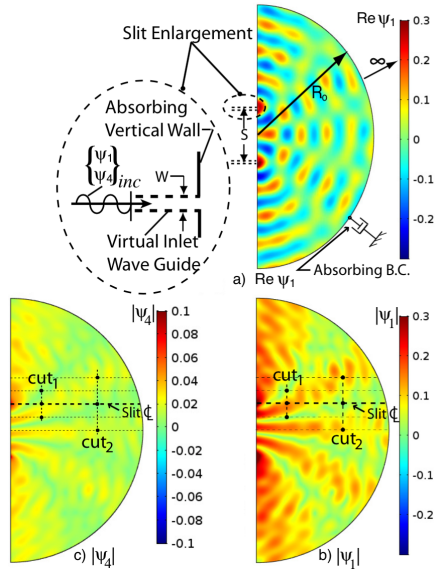
Figure 7 Interference of Dirac Wave Passing Through 2 Slits: (a) Real Part ψ_1, (b) Mag. $|\psi_1|$, (c) Mag. $|\psi_4|$

facing absorber is used on the inside vertical wall of the FEM domain to absorb spurious reflections from any imperfections in the outer boundary absorbing B.C. . With sect. 5.1 parameters, the FEM solution is in Fig.(7), where Fig.(7a) shows the Real Part ψ_1 and Figs.(7b) & (7c) show the Mag. $|\psi_1|$, $|\psi_4|$. Observe waves emerging from the slits interact, forming bands of orange constructive and green destructive interference. In close at Fig.(7b) cut-1, the Eq. (20) probability density $\rho'(x,y)$ is 0.067 times smaller @ $\Delta y=\lambda/2$ above the slit than in line with the slit, and 0.037 times smaller @ $\Delta y=-\lambda/2$ below the slit than in line with the slit (locations

denoted by •). One might intuitively expect the cut-1 $\rho'(x,y)$ to be greater in line with the slit. Yet farther back at cut-2, $\rho'(x,y)$ is 18.9 times bigger @ $\Delta y=\lambda$ above the slit than in line with the slit and 22.1 times bigger @ $\Delta y=-\lambda$ below the slit than in line with the slit. It is unintuitive to have $\rho'(x,y)$ be greater not in line with the slit, and this effect is due to the constructive interference.
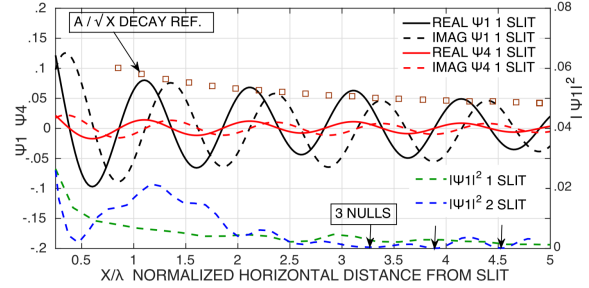
Figure 8 No Wave Interference with Bottom Slit Shut

In Fig.(8), with bottom slit shut, ψ_m is plotted on the top slit centerline where the real and imag. parts of ψ_m have a traveling wave structure and fall off like $1/\sqrt{x}$ cyl. wave spreading. Three interference nulls for the 2-slit run ($|\psi_1|^2$ blue $--$ plots) are shown compared to a 1-slit shut run ($|\psi_1|^2$ green $--$ plots) without interference nulls.

7. Conclusions

Agreement between the exact vs FEM solution for three validation examples is good. Solutions to the incident harmonic wave upon a two slit barrier, produced diffraction patterns showing bands of null zones due to wave destructive interference, thus showing the diffraction behavior of particles at the atomic scale. Dirac equations are spatially 1st order, thus truncated infinite domains with absorbing B.C.'s work but explicit downstream B.C.'s on ψ_m should be avoided. Future work is needed for higher order absorbing B.C.'s (e.g. perfectly matched layers) than the first order plane wave ones used here.

8. References

[1] Paul Strange, Relativistic Quantum Mechanics, Camb. Univ. Press Cambridge 1998.

[2] E. Pozdeeva , A.Schulze-Halberg ,"Darboux Transformation ", J. Math. Phys. **51** (2010).

[3] G.F. Torres, et al., "Solution of Nonscaler Eqs." ,Revista Mex. de Fisica **38**, No 1 (1992).

[4] A.J. Kalinowski, "Quantum Mechanics Applications" ,COMSOL Conf. Proc, 2015.